

Prospects for topologically non-trivial electronic and magnetic states in correlated kagome lattice materials

Daniel Guterding,* Harald O. Jeschke, and Roser Valentí
*Institut für Theoretische Physik, Goethe-Universität Frankfurt,
 Max-von-Laue-Straße 1, 60438 Frankfurt am Main, Germany*

We investigate possible realizations of the quantum spin Hall effect (QSHE), the quantum anomalous Hall effect (QAHE) and quantum spin-liquids (QSL) in doped copper kagome materials based on natural minerals Herbertsmithite $[\text{ZnCu}_3(\text{OH})_6\text{Cl}_2]$ and Barlowite $[\text{Cu}_4(\text{OH})_6\text{FBr}]$. Using *ab-initio* density functional theory calculations we estimate the stability of the hypothetical materials against structural distortions and analyze their electronic and magnetic properties. We find that materials based on Herbertsmithite show non-trivial band-topology and propose candidates for the QSHE at filling $4/3$ and the QAHE at filling $2/3$. Furthermore, we point out a route to realize a QSL based on the Barlowite system.

PACS numbers: 71.20.-b, 73.43.-f, 75.10.Jm, 75.30.Et

The possible experimental realization of quantum spin-liquids (QSL) based on spin-1/2 kagome lattices has generated in the past intense research efforts on Herbertsmithite and similar frustrated antiferromagnets [1–11]. Recently, chemical doping of Herbertsmithite was proposed as a way to obtain a strongly correlated Dirac-kagome metal with frustrated magnetic interactions [12]. Such a material could realize exotic states of matter such as unconventional superconductivity or weak ferromagnetism at intermediate electron doping [12], where the Dirac point and van Hove singularities of the kagome lattice could be accessed [13].

A problem in Herbertsmithite and related materials is the intrinsic disorder [14–16], which might prevent the formation of a quantum spin-liquid. Recently, the geometrically perfect spin-1/2 kagome antiferromagnet Barlowite was discovered [17–19]. It is closely related to Herbertsmithite, but features magnetic ions on interplane sites, which couple the kagome planes magnetically and lead to magnetic ordering at low temperatures [19]. Therefore, selective doping of non-magnetic ions into those interplane sites could be a way to realize a quantum spin-liquid [19].

Recently, systems with a kagome lattice have also received considerable attention because they potentially realize quasiparticle bands with non-trivial topology [20–23]. From topologically non-trivial electronic bands, effects such as the Quantum Spin Hall effect (QSHE) [24, 25] and the Quantum Anomalous Hall effect (QAHE) [26] can emerge. Realizations of the latter are intensively sought for, because dissipation-free, spin-polarized edge currents in absence of external magnetic fields, as manifested in the QAHE, have tremendous potential for application in new energy-efficient spintronic devices [27, 28]. So far, the QAHE has only been observed in thin films of chromium-doped $(\text{Bi,Sb})_2\text{Te}_3$ at a temperature of 30 mK [29, 30]. Meanwhile, it has been proposed that the QAHE can be realized in some other materials, e.g. by means of manipulated surfaces [23, 31, 32].

In the context of transition-metal-based kagome systems, like Herbertsmithite, these exotic states of matter have hardly ever been considered. Based on *ab-initio* density functional theory (DFT) calculations we show that a number of materials derived from Herbertsmithite possess non-trivial band-topology. In particular, we predict that the QAHE can be realized in hole-doped compounds for a filling $n = 2/3$ corresponding to the flat band region in the pure kagome lattice (see Fig. 1). In contrast, electron-doped materials should show a QSHE at a filling $n = 4/3$ where the pure kagome lattice has a Dirac point (see Fig. 1). Evaluating DFT total energies, we thoroughly check possibilities for structural distortions to ensure that single crystals of the materials of interest can in principle be synthesized.

In addition to the results on doped Herbertsmithite, we also identify the most promising dopant atoms for realizing a QSL state in substituted Barlowite. Previous

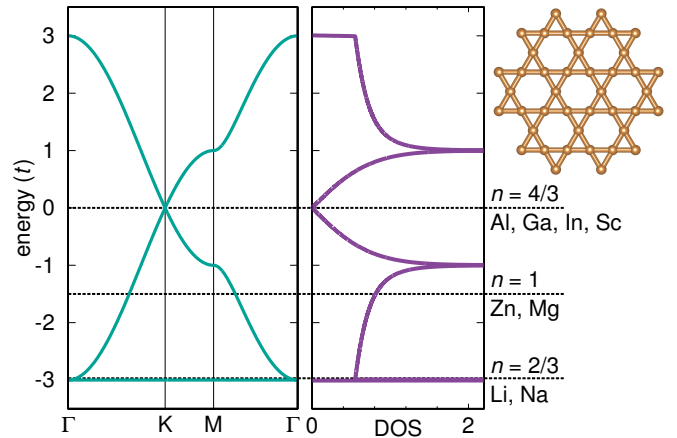


FIG. 1. (Color online) Electronic bandstructure and density of states (DOS) of the pure kagome lattice. On the right hand side the possible substituent elements for the Herbertsmithite system with corresponding Fermi level are listed.

suggestions for stable modifications of Barlowite were based on the evaluation of doping energies in large supercells [33]. We also consider the possibility that substitution distorts the shape of the unit cell and therewith destroys the perfect kagome motif. We show that only a few substituents leave the kagome motif undistorted.

Total energies, electronic bandstructures and magnetic exchange interactions were evaluated using *ab-initio* density functional theory (DFT) calculations within an all-electron full-potential local orbital (FPLO) [34] basis. For the exchange-correlation functional we employed the generalized gradient approximation (GGA) [35], as well as GGA+U [36] functionals. The Hubbard repulsion on the Cu 3d orbitals was set to $U = 6$ eV and Hund's rule coupling to $J_H = 1$ eV. Additionally, we investigated the effect of spin-orbit coupling (SOC) on the electronic bandstructure using the full-relativistic version of the FPLO code. Total energies, electronic bandstructures, tight-binding models and Heisenberg models were extracted from calculations converged using 8^3 , 20^3 , 40^3 and 6^3 k -point grids respectively.

Experimental and hypothetical crystal structures were fully relaxed using the projector augmented wave (PAW) method [37] implemented in GPAW [38] with a plane-wave cutoff of 1000 eV and the GGA exchange-correlation functional [35]. We optimized the stoichiometric structures of Herbertsmithite-based compounds using 6^3 k -points (4^3 k -points for compounds based on Barlowite and non-stoichiometric structures) until forces were below 10 meV/Å.

Hypothetical crystal structures were prepared starting from the experimental crystal structure of Herbertsmithite [1], substituting zinc (Zn^{2+}) atoms between the copper kagome layers by monovalent $A=\text{Li}^+$, Na^+ (hole-doping), divalent Mg^{2+} (isoelectronic), and trivalent Al^{3+} , Ga^{3+} , In^{3+} , Sc^{3+} , Y^{3+} (electron-doping). We refer to these compounds as A -Herbertsmithite, $\text{ACu}_3(\text{OH})_6\text{Cl}_2$.

For each of these materials we also constructed a defect structure, where we lowered the symmetry of the unit cell and exchanged the substituent A with a copper atom from a kagome lattice site. As the chemical composition of these defect structures is identical to the defect-free structures, energy differences can be evaluated directly within DFT. In case the defect structure has lower energy, the kagome lattice is likely to be destroyed and the phenomena of interest here will not arise in the target compound. To further analyse the phase stability, we also evaluated total energies of $3 \times 1 \times 1$ supercells with A -site vacancies or copper impurities on the interlayer site. For Herbertsmithite and Mg-Herbertsmithite we also considered smaller concentrations of copper impurities on the interlayer site as well as of dopant impurities introduced into the kagome plane using $3 \times 2 \times 1$ supercells. Furthermore, we investigated the $\text{Ga}_x\text{Zn}_{1-x}\text{Cu}_3(\text{OH})_6\text{Cl}_2$ doping series. Formation and doping energies are calculated

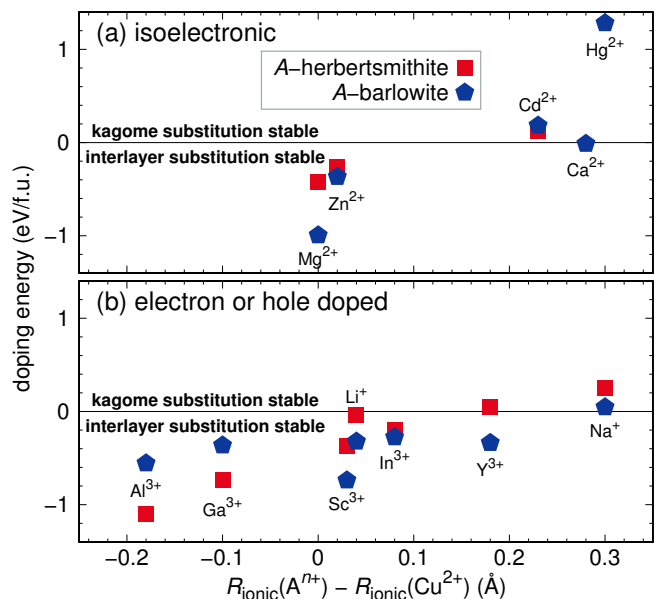


FIG. 2. (Color online) Calculated doping energies for Herbertsmithite and Barlowite. All data points above the zero line indicate that the kagome lattice will be distorted upon doping. On the interlayer site, both Herbertsmithite and Barlowite prefer to incorporate ions with smaller radius than Cu^{2+} . Ionic radii in coordination number 6 are taken from Ref. 40.

TABLE I. Calculated doping energies in eV (electron volts) per formula unit of Herbertsmithite or Mg-Herbertsmithite $[\text{ACu}_3(\text{OH})_6\text{Cl}_2]$, $A = \text{Zn}, \text{Mg}$. Negative values signal stability of the stoichiometric compound against the formation of copper impurities on the interlayer site (top line) and formation of dopant impurities in the kagome plane (bottom line).

$A =$	Zn^{2+}	Mg^{2+}
$A_{0.83}\text{Cu}_{3.17}(\text{OH})_6\text{Cl}_2$	-0.464	-0.831
$A_{1.17}\text{Cu}_{2.83}(\text{OH})_6\text{Cl}_2$	+0.210	+0.803

from DFT(GGA) total energies in the solid state. Details are given in Ref. 39.

For Barlowite we started from the experimental crystal structure [17] and substituted the interlayer copper site (Cu^{2+}) by $A=\text{Li}^+$, Na^+ , Mg^{2+} , Zn^{2+} , Al^{3+} , Ga^{3+} , In^{3+} , Sc^{3+} , Y^{3+} , forming A -substituted Barlowite, $\text{ACu}_3(\text{OH})_6\text{FBr}$. Again we checked whether the dopant atoms prefer to occupy a kagome lattice site rather than an interlayer site. Isoelectronic doping with $A=\text{Ca}^{2+}$, Cd^{2+} , Hg^{2+} is included for completeness.

In Fig. 2 we plot the energy difference between substitution at the kagome site and substitution at the interlayer site for Herbertsmithite and Barlowite as a function of the substituent ionic radius [40]. In Herbertsmithite, sodium (Na^+) and yttrium (Y^{3+}) prefer to occupy a site in the kagome layer, which generates a monoclini-

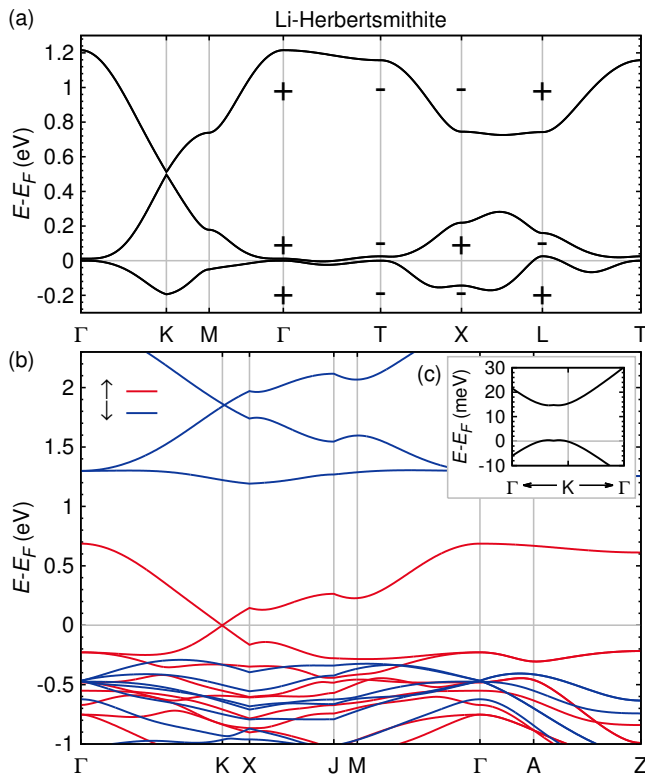


FIG. 3. (Color online) (a) Full-relativistic non-spin-polarized bandstructure of Li-Herbertsmithite. Plus and minus signs denote the parities of the three bands closest to the Fermi level at eight inversion-symmetric points (Γ , $3 \times T$, $3 \times L$, T) in the Brillouin zone. (b) FM bandstructure of Li-Herbertsmithite without SOC. The spin down channel is gapped, while the Dirac point of the spin up channel is located exactly at the Fermi level. The path through the Brillouin zone is equivalent to the one chosen in Ref. 12. (c) Full-relativistic FM bandstructure of Li-Herbertsmithite close to the Dirac point. SOC opens a gap.

cally distorted crystal structure with no perfect kagome lattice. If the substituent atom occupies the interlayer site, the perfect kagome motif is preserved. In experiment, Cd^{2+} -substituted Herbertsmithite assumes a crystal structure with buckled kagome layers and Cd^{2+} ions between those layers [41]. In our calculations, we do not investigate this type of defect structures, but we correctly reproduce that substitution with Cd^{2+} destroys the perfect kagome lattice. For Herbertsmithite and iso-electronic Mg-Herbertsmithite we find a clear tendency to form impurities of zinc (Zn^{2+}) and magnesium (Mg^{2+}) in the kagome plane (see Table I). These results are in agreement with previous experimental reports [14, 15], but seem to contradict the interpretation of recent experimental investigations on Herbertsmithite [16]. More work is needed to understand the antisite disorder in Herbertsmithite. Mg-Herbertsmithite appears nonetheless to be more prone to defects in the kagome layer than Herbertsmithite.

In terms of substitution energies, aluminum (Al^{3+}), gallium (Ga^{3+}) and scandium (Sc^{3+}) are the most promising candidates for synthesis of electron-doped Herbertsmithite. On the hole-doped side, lithium (Li^+) is a promising candidate for substitution. Formation of the substituted materials is found to be energetically favorable compared to the formation of Clinoatacamite, $\text{Cu}_2(\text{OH})_3\text{Cl}$. All Herbertsmithite-based materials investigated are stable against formation of vacancies and copper impurities, as opposed to full substitution, on the interlayer site. The doping series $\text{Ga}_x\text{Zn}_{1-x}\text{Cu}_3(\text{OH})_6\text{Cl}_2$ should be stable in a broad substitution range [39].

In the analysis of the electronic and magnetic properties we concentrate first on the hole-doped materials ($n = 2/3$) where the Fermi level lies in the region of the flat band of the kagome lattice (see Fig. 1) and a strong ferromagnetic instability is to be expected. Fig. 3 (a) shows the full-relativistic non-spin-polarized electronic bandstructure of Li-Herbertsmithite, where the parities of the three bands closest to the Fermi level are also indicated. Due to the bulk nature of the system, the ideal kagome flat band acquires some dispersion. Nonetheless, ferromagnetism is strongly favored. Indeed, total energy calculations of Li-Herbertsmithite in various copper spin configurations give ferromagnetism as the ground state.

Furthermore, parametrizing the Cu-Cu interactions by mapping GGA+U total energies to a spin-1/2 Heisenberg Hamiltonian shows a large ferromagnetic next-neighbor exchange $J_1 = 544$ K and other couplings with magnitude smaller than $0.1J_1$ (see Ref. 39). Using a mean-field approximation [42], we estimate a Curie temperature of $T_C \approx 1160$ K.

Fig. 3 (b) displays the non-relativistic ferromagnetic bandstructure obtained with the GGA+U functional. The Fermi level of the majority bands lies right at the Dirac point [43] and inclusion of spin-orbit coupling opens a gap (see inset in Fig. 3).

Non-trivial band-topology has so far been ignored entirely in the Herbertsmithite system. We have calculated the product of parity eigenvalues at eight inversion-symmetric points (see Fig. 3) in the Brillouin zone (Γ , $3 \times T$, $3 \times L$, T) [44]. For all materials of the Herbertsmithite family, topological numbers of the bands below the Dirac point are $\nu_0; (\nu_1, \nu_2, \nu_3) = 0; (111)$. Therefore, the system realizes a stack of two-dimensional topological insulators (so-called *weak* TI), which displays conducting states on a (001) surface [44], although the bulk bands are gapped by relativistic effects. Note that non-trivial band topology is intrinsic to the perfect kagome lattice [45, 46] and no particular inversion of orbital weights is required unlike in most topological insulators [29, 47]. In real materials however, the kagome layer is embedded into a crystal, where non-trivial band-topology can be destroyed by additional hybridizations. We observe this case for all materials derived from Barlowite that we investigated here.

Having found non-trivial band-topology in the Herbertsmithite system, we predict that hole-doped Herbertsmithite shows a QAHE at $n = 2/3$ filling while electron-doped Herbertsmithite shows a QSHE at $n = 4/3$ filling. In the latter case, the Fermi level of the non-spin-polarized bandstructure lies right at the Dirac point (see Fig. 1). To demonstrate the existence of surface states in these two cases, we constructed tight-binding models for the copper states $(n, j, m_j) = (3, 5/2, \pm 5/2)$ from full-relativistic DFT calculations using projective Wannier functions [48]. Employing a method based on Green's functions [49–51], we calculate the states on the (001) plane of semi-infinite interlayer-substituted Herbertsmithite. The lattice plane refers to the unit cell in rhombohedral setting of space group $R\bar{3}m$. Explicitly, we take into account 10^5 layers parallel to the surface. In the Green's functions $G(k, \omega)$ with energy ω and momentum k we introduce an artificial broadening of 0.01 meV to ensure numerical convergence. We terminate the edges of the kagome layers with chains of atoms as shown in the inset of Fig. 4 (a). The obtained spectral function $A(k, \omega) = -\text{Im} G(k, \omega)/\pi$ of the surface layer in chain termination is shown in Fig. 4, where the k -path is chosen perpendicular to the direction in which surface states propagate. The hole-doped case clearly shows only one surface state crossing the Fermi level [QAHE, see Fig. 4 (a)], while the electron-doped case shows two [QSHE, see Fig. 4 (b)]. The spectral function of the dual surface (triangles termination) has the same essential features and is included in Ref. 39. As we take into account realistic bandstructures, our spectral functions show additional structure away from the Fermi level compared to model calculations in next-neighbor approximation [45, 46].

We proceed now with Barlowite and the possibility of realizing quantum spin liquid systems. Doping energies of substituted Barlowite are shown in Fig. 2. We find that Barlowite has a strong preference for dopant atoms with ionic radii similar to copper, like zinc (Zn^{2+}) and magnesium (Mg^{2+}) at the interlayer position. For Mg^{2+} , the energy difference between doping into the kagome layer and doping onto the interlayer site is much larger than in Herbertsmithite (see Fig. 2), which indicates that site-disorder is likely to be significantly reduced in the Barlowite system.

We identify Mg-substituted Barlowite as the most promising candidate for a QSL material. We estimate exchange constants by mapping GGA+U total energies to a spin-1/2 Heisenberg Hamiltonian and find that the system can be described by two antiferromagnetic couplings J_i , the next-neighbor coupling on the kagome lattice $J_1 = 226$ K and the interlayer coupling $J_2 = 13.4$ K, with a ratio $J_2/J_1 = 0.06$. All other exchange constants are smaller than 2 K. Therefore, Mg-Barlowite is described by a much simpler Hamiltonian than Herbertsmithite [5]. Recent theoretical calculations predict a

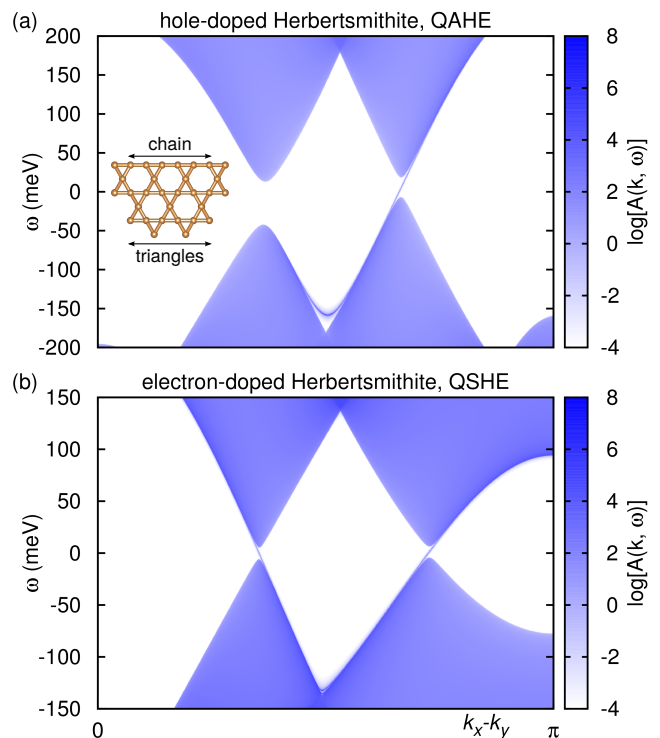


FIG. 4. (Color online) States on the (001) surface of (a) Li-Herbertsmithite (hole-doped) and (b) Ga-Herbertsmithite (electron-doped) calculated using Green's functions for the semi-infinite system. The inset of (a) shows the two possible terminations of the kagome lattice.

spin-liquid ground state to be realized in the corresponding Heisenberg model for $|J_2/J_1| < 0.15$ [52].

In this work we have suggested some examples of materials that merge non-trivial band topology with correlation effects. We have shown that substituting Herbertsmithite with alkali, transition or group 13 metal ions promises realizations of the Quantum Spin Hall effect upon integer electron-doping (scandium, aluminum, gallium, indium) and Quantum Anomalous Hall effect upon integer hole-doping (lithium). In the intermediate electron-doping regime, the Fermi level can be tuned continuously by preparing solid solutions of different dopant atoms. Therefore, fillings close to 4/3, where exotic ferromagnetism and unconventional superconductivity have been predicted, should be accessible experimentally. For Barlowite we have shown that substitution with magnesium will likely yield a Quantum Spin Liquid material with site-disorder significantly reduced compared to Herbertsmithite.

The QAHE predicted for hole-doped Herbertsmithite as well as the QSL predicted for isoelectronic doped Barlowite are only possible due to the correlated nature of the Cu d -orbitals. In the former case, electron-electron correlation leads to the existence of fully spin-polarized Cu d -bands with a gap to the empty minority bands,

while in the latter case correlations are responsible for the Mott insulating nature of the system, where a QSL state could be realized. Studies beyond DFT would be desirable and will be pursued in the future.

The authors thank Kira Riedl, Milan Tomić, Bernd Wolf, Pascal Puphal, Cornelius Krellner, Hans Boschker, Jochen Mannhart, Martin Jansen and Claudia Felser for fruitful discussions and gratefully acknowledge support by the Deutsche Forschungsgemeinschaft through grant SFB/TR 49. RV was supported in part by the Kavli Institute for Theoretical Physics at the University of California, Santa Barbara under National Science Foundation grant No. PHY11-25915.

* guterding@itp.uni-frankfurt.de

- [1] M. P. Shores, E. A. Nytko, B. M. Bartlett, and D. G. Nocera, *A Structurally Perfect $S=1/2$ Kagomé Antiferromagnet*, J. Am. Chem. Soc. **127**, 13462 (2005).
- [2] P. Mendels and F. Bert, *Quantum Kagome Antiferromagnet $ZnCu_3(OH)_6Cl_2$* , J. Phys. Soc. Jpn. **79**, 011001 (2010).
- [3] P. Mendels and F. Bert, *Quantum Kagome Antiferromagnet: $ZnCu_3(OH)_6Cl_2$* , J. Phys. Conf. Ser. **320**, 012004 (2011).
- [4] R. H. Colman, A. Sinclair, and A. S. Willis, *Comparisons between Haydeeite, $\alpha-Cu_3Mg(OD)_6Cl_2$, and Kapellasite, $\alpha-Cu_3Zn(OD)_6Cl_2$, Isostructural $S = 1/2$ Kagome Magnets*, Chem. Mater. **22**, 5774 (2010).
- [5] H. O. Jeschke, F. Salvat-Pujol, and R. Valentí, *First-principles determination of Heisenberg Hamiltonian parameters for the spin-1/2 kagome antiferromagnet $ZnCu_3(OH)_6Cl_2$* , Phys. Rev. B **88**, 075106 (2013).
- [6] Y. Li, B. Pan, S. Li, W. Tong, L. Ling, Z. Yang, J. Wang, Z. Chen, Z. Wu, and Q. Zhang, *Gapless quantum spin liquid in the $S = 1/2$ anisotropic kagome antiferromagnet $ZnCu_3(OH)_6SO_4$* , New J. Phys. **16**, 093011 (2014).
- [7] Y. Li and Q. Zhang, *Structure and magnetism of $S = 1/2$ kagome antiferromagnets $NiCu_3(OH)_6Cl_2$ and $CoCu_3(OH)_6Cl_2$* , J. Phys.: Condens. Matter **25**, 026003 (2013).
- [8] T.-H. Han, J. S. Helton, S. Chu, D. G. Nocera, J. A. Rodriguez-Rivera, C. Broholm, and Y. S. Lee, *Fractionalized excitations in the spin-liquid state of a kagome-lattice antiferromagnet*, Nature **492**, 406 (2012).
- [9] R. H. Colman, A. Sinclair, and A. S. Willis, *Magnetic and Crystallographic Studies of Mg-Herbertsmithite, $\gamma-Cu_3Mg(OH)_6Cl_2$ – A new $S = 1/2$ Kagome Magnet and Candidate Spin Liquid*, Chem. Mater. **23**, 1811 (2011).
- [10] B. Bauer, L. Cincio, B. P. Keller, M. Dolfi, G. Vidal, S. Trebst, and A. W. W. Ludwig, *Chiral spin liquid and emergent anyons in a Kagome lattice Mott insulator*, Nat. Commun. **5**, 5137 (2014).
- [11] Y.-C. He, D. N. Sheng, and Y. Chen, *Obtaining topological degenerate ground states by the density matrix renormalization group*, Phys. Rev. B **89**, 075110 (2014).
- [12] I. I. Mazin, H. O. Jeschke, F. Lechermann, H. Lee, M. Fink, R. Thomale, and R. Valentí, *Theoretical prediction of a strongly correlated Dirac metal*, Nat. Commun. **5**, 4261 (2014).
- [13] T. Hanisch, G. Uhrig, and E. Müller-Hartmann, *Lattice dependence of saturated ferromagnetism in the Hubbard model*, Phys. Rev. B **56**, 13690 (1997).
- [14] S.-H. Lee, H. Kikuchi, Y. Qiu, B. Lake, Q. Huang, K. Habicht, and K. Kiefer, *Quantum-spin-liquid states in the two-dimensional kagome antiferromagnets $Zn_xCu_{4-x}(OD)_6Cl_2$* , Nat. Mater. **6**, 853 (2007).
- [15] M. A. de Vries, K. V. Kamenev, W. A. Kockelmann, J. Sanchez-Benitez, and A. Harrison, *Magnetic Ground State of an Experimental $S = 1/2$ Kagome Antiferromagnet*, Phys. Rev. Lett. **100**, 157205 (2008).
- [16] D. E. Freedman, T. H. Han, A. Prodi, P. Müller, Q.-Z. Huang, Y.-S. Chen, S. M. Webb, Y. S. Lee, T. M. McQueen, and D. G. Nocera, *Site Specific X-ray Anomalous Dispersion of the Geometrically Frustrated Kagomé Magnet, Herbertsmithite $ZnCu_3(OH)_6Cl_2$* , J. Am. Chem. Soc **132**, 16185 (2010).
- [17] P. Elliott and M. A. Cooper, *Barlowite, $Cu_4FBr(OH)_6$, a new mineral isostructural with claringbullite: description and crystal structure*, Mineralog. Mag. **78**, 1755 (2014).
- [18] T.-H. Han, J. Singleton, and J. A. Schlueter, *Barlowite: A Spin-1/2 Antiferromagnet with a Geometrically Perfect Kagome Motif*, Phys. Rev. Lett. **113**, 227203 (2014).
- [19] H. O. Jeschke, F. Salvat-Pujol, E. Gati, N. H. Hoang, B. Wolf, M. Lang, J. A. Schlueter, and R. Valentí, *Barlowite as a canted antiferromagnet: Theory and experiment*, Phys. Rev. B **92**, 094417 (2015).
- [20] A. Mook, J. Henk, and I. Mertig, *Edge states in topological magnon insulators*, Phys. Rev. B **90**, 024412 (2014).
- [21] M. Pereiro, D. Yudin, J. Chico, C. Etz, O. Eriksson, and A. Bergman, *Topological excitations in a kagome magnet*, Nat. Commun. **5**, 4815 (2014).
- [22] R. Chisnell, J. S. Helton, D. E. Freedman, D. K. Singh, R. I. Bewley, D. G. Nocera, and Y. S. Lee, *Topological Magnon Bands in a Kagome Lattice Ferromagnet*, Phys. Rev. Lett. **115**, 147201 (2015).
- [23] G. Xu, B. Lian, and S.-C. Zhang, *Intrinsic Quantum Anomalous Hall effect in Kagome lattice $Cs_2LiMn_3F_{12}$* , Phys. Rev. Lett **115**, 186802 (2015).
- [24] C. L. Kane and E. J. Mele, *Quantum Spin Hall Effect in Graphene*, Phys. Rev. Lett. **95**, 226801 (2005).
- [25] B. A. Bernevig and S.-C. Zhang, *Quantum Spin Hall Effect*, Phys. Rev. Lett. **96**, 106802 (2006).
- [26] F. D. M. Haldane, *Model for a Quantum Hall Effect without Landau Levels: Condensed-Matter Realization of the "Parity Anomaly"*, Phys. Rev. Lett. **61**, 2015 (1988).
- [27] K. He, *The Quantum Hall Effect Gets More Practical*, Physics **8**, 41 (2015).
- [28] see for a review: H. Weng, R. Yu, X. Hu, X. Dai, and Z. Fang, *Quantum anomalous Hall effect and related topological electronic states*, Adv. Phys. **64**, 227 (2015).
- [29] R. Yu, W. Zhang, H.-J. Zhang, S.-C. Zhang, X. Dai, and Z. Fang, *Quantized Anomalous Hall Effect in Magnetic Topological Insulators*, Science **329**, 61 (2010).
- [30] C.-Z. Chang, J. Zhang, X. Feng et al., *Experimental Observation of the Quantum Anomalous Hall Effect in a Magnetic Topological Insulator*, Science **340**, 167 (2013).
- [31] K. F. Garrity and D. Vanderbilt, *Chern Insulators from Heavy Atoms on Magnetic Substrates*, Phys. Rev. Lett. **110**, 116802 (2013).
- [32] S.-C. Wu, G. Shang, and B. Yan, *Prediction of Near-Room-Temperature Quantum Anomalous Hall Effect on Honeycomb Materials*, Phys. Rev. Lett. **113**, 256401 (2014).

- [33] Z. Liu, X. Zou, J.-W. Mei, and F. Liu, *Selective doping Barlowite for quantum spin liquid: a first-principles study*, arXiv:1504.00521 (unpublished).
- [34] K. Koepnik and H. Eschrig, *Full-potential nonorthogonal local-orbital minimum-basis band-structure scheme*, Phys. Rev. B **59**, 1743 (1999); <http://www.FPLO.de>
- [35] J. P. Perdew, K. Burke, and M. Ernzerhof, *Generalized Gradient Approximation Made Simple*, Phys. Rev. Lett. **77**, 3865 (1996).
- [36] A. I. Liechtenstein, V. I. Anisimov, and J. Zaanen, *Density-functional theory and strong interactions: Orbital ordering in Mott-Hubbard insulators*, Phys. Rev. B **52**, R5467(R) (1995).
- [37] P. E. Blöchl, *Projector augmented-wave method*, Phys. Rev. B **50**, 17953 (1994).
- [38] J. Enkovaara, C. Rostgaard, J. J. Mortensen *et al.*, *Electronic structure calculations with GPAW: a real-space implementation of the projector augmented-wave method*, J. Phys.: Condens. Matter **22**, 253202 (2010); <https://wiki.fysik.dtu.dk/gpaw>
- [39] See Supplemental Material at [URL inserted by publisher], which discusses several other types of possible defect structures for materials based on Herbertsmithite and includes tabulated values for all formation and doping energies calculated. Additionally, we provide an analysis of the $\text{Ga}_x\text{Zn}_{1-x}\text{Cu}_3(\text{OH})_6\text{Cl}_2$ doping series and document the formalism we use to compute the surface states. We explain the parametrization of exchange couplings within a Heisenberg model for Li-Herbertsmithite and Mg-Barlowite. Furthermore, we estimate the Curie temperature of Li-Herbertsmithite.
- [40] R. D. Shannon, *Revised Effective Ionic Radii and Systematic Studies of Interatomic Distances in Halides and Chalcogenides*, Acta Cryst. A **32**, 751 (1976).
- [41] T. M. McQueen, T. H. Han, D. E. Freedman, P. W. Stephens, Y. S. Lee, and D. G. Nocera, *$\text{CdCu}_3(\text{OH})_6\text{Cl}_2$: A new layered hydroxide chloride*, J. Solid State Chem. **184**, 3319 (2011).
- [42] S. Blundell, *Magnetism in Condensed Matter* (Oxford University Press, Oxford, 2010).
- [43] The Dirac point position is slightly displaced from K due to the finite coupling between the kagome layers, as has been observed previously in Ref. 12.
- [44] L. Fu and C. L. Kane, *Topological insulators with inversion symmetry*, Phys. Rev. B **76**, 045302 (2007).
- [45] Z. Wang and P. Zhang, *Quantum spin Hall effect and spin-charge separation in a kagomé lattice*, New J. Phys. **12**, 043055 (2010).
- [46] Z.-Y. Zhang, *The quantum anomalous Hall effect in kagomé lattices*, J. Phys.: Condens. Matter **23**, 365801 (2011).
- [47] L. Zhou, K. Kou, Y. Sun, C. Felser, F. Hu, G. Shan, S. C. Smith, B. Yan, and T. Frauenheim, *New Family of Quantum Spin Hall Insulators in Two-dimensional Transition-Metal Halide with Large Nontrivial Band Gaps*, arXiv:1510.06090 (unpublished).
- [48] H. Eschrig and K. Koepnik, *Tight-binding models for the iron-based superconductors*, Phys. Rev. B **80**, 104503 (2009).
- [49] M. P. López Sancho, J. M. López Sancho, and J. Rubio, *Quick iterative scheme for the calculation of transfer matrices: application to $\text{Mo}(100)$* , J. Phys. F: Met. Phys. **14**, 1205 (1984).
- [50] M. P. López Sancho, J. M. López Sancho, and J. Rubio, *Highly convergent schemes for the calculation of bulk and surface Green functions*, J. Phys. F: Met. Phys. **15**, 851 (1985).
- [51] X. Dai, T. L. Hughes, X.-L. Qi, Z. Fang, and S.-C. Zhang, *Helical edge and surface states in HgTe quantum wells and bulk insulators*, Phys. Rev. B **77**, 125319 (2008).
- [52] O. Götze and J. Richter, *The route to magnetic order in the spin-1/2 kagome Heisenberg antiferromagnet: The role of interlayer coupling*, arXiv:1510.04898 (unpublished).

Prospects for topologically non-trivial electronic and magnetic states in correlated kagome lattice materials: Supplemental Information

Daniel Guterding,* Harald O. Jeschke, and Roser Valentí
*Institut für Theoretische Physik, Goethe-Universität Frankfurt,
 Max-von-Laue-Straße 1, 60438 Frankfurt am Main, Germany*

I. FORMATION AND DOPING ENERGIES

Total energies were evaluated using *ab-initio* density functional theory (DFT) calculations within an all-electron full-potential local orbital (FPLO)¹ basis. For the exchange-correlation functional we employ the generalized gradient approximation (GGA)². Total energies were extracted from calculations converged using 8^3 k -point grids.

Experimental and hypothetical crystal structures were fully relaxed using the projector augmented wave (PAW) method³ implemented in GPAW⁴ with a plane-wave cutoff of 1000 eV and the GGA exchange-correlation functional². We optimized the stoichiometric structures of Herbertsmithite-based compounds using 6^3 k -points (4^3 k -points for compounds based on Barlowite and non-stoichiometric structures) until forces were below 10 meV/Å.

Hypothetical crystal structures were prepared starting from the experimental crystal structure of Herbertsmithite⁵, substituting zinc (Zn) atoms between the copper kagome layers by monovalent $A=\text{Li, Na}$ (hole-doping), divalent Mg (isoelectronic), and trivalent Al, Ga, In, Sc, Y (electron-doping). We refer to these compounds as A -Herbertsmithite, $\text{ACu}_3(\text{OH})_6\text{Cl}_2$ (case 1) and estimate their stability by comparison to Clinoatcamite $[\text{Cu}_2(\text{OH})_3\text{Cl}]$. We directly compare energies of A -substituted materials, where the dopant sits in the interlayer site versus structures where it occupied a kagome site (case 2, see Fig. 2 in main paper). To analyse the phase stability, we also evaluate total energies of $3 \times 1 \times 1$ supercell structures, where either one of the A -sites is vacant $[\text{A}_{0.66}\text{Cu}_3(\text{OH})_6\text{Cl}_2]$, case 3) or occupied by a Cu impurity $[\text{A}_{0.66}\text{Cu}_{3.33}(\text{OH})_6\text{Cl}_2]$, case 4).

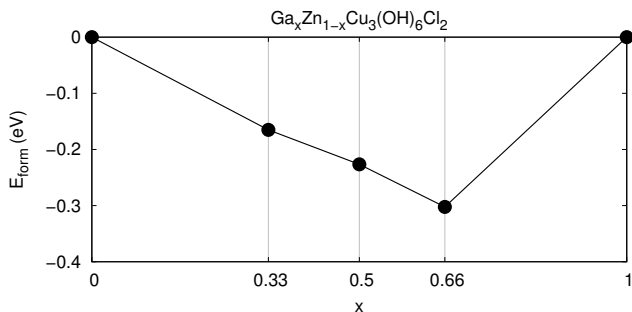


FIG. 1. Formation energies of the $\text{Ga}_x\text{Zn}_{1-x}\text{Cu}_3(\text{OH})_6\text{Cl}_2$ doping series. Lines are guides to the eye.

To analyze whether the presence of excess copper in the synthesis process makes the formation of Clinoatcamite favorable compared to $\text{ACu}_3(\text{OH})_6\text{Cl}_2$, we compare the total energies of Cu in a copper crystal plus the energy of $\text{ACu}_3(\text{OH})_6\text{Cl}_2$ to the total energy of A in a crystal of substance A plus the total energy of Clinoatcamite. Proper normalization of total energies to formula units is taken into account. The calculated energy difference determines whether the formation of metallic patches of substance A is energetically favourable compared to forming A -substituted Herbertsmithite. The formation energy for this case is defined as

$$E_{\text{form}} = E_{\text{Cu}} + E_{\text{AH}} - (E_A + E_C), \quad (1)$$

where E_A refers to the pure crystalline metal A , E_{AH} to A -Herbertsmithite and E_C to Clinoatcamite. As all total energies are negative, a negative formation energy signals stability of the target compound $\text{ACu}_3(\text{OH})_6\text{Cl}_2$. As a consistency check, we also prepared a structure with copper on the interlayer site so that the chemical formula is identical to Clinoatcamite. For this structure, we find a positive formation energy. Therefore, hypothetical Cu-Herbertsmithite is unstable with respect to the formation of Clinoatcamite, as expected. The evaluation of formation energies for substituted Barlowite⁶ is done analogously.

For the formation energy of impurity or vacancy structures, we use

$$E_{\text{form}} = y \cdot E_{\text{Cu}} + E_{\text{AH}} - (x \cdot E_A + E_{\text{AHM}}), \quad (2)$$

where E_{AHM} is the total energy of the compound $\text{A}_{1-x}\text{Cu}_{3+y}(\text{OH})_6\text{Cl}_2$.

Formation energies for modifications of Herbertsmithite are shown in Table I. As all calculated energy differences are negative, formation of A -Herbertsmithite is always favorable compared to formation of Clinoatcamite. All proposed modifications are robust against formation of vacancies or copper impurities on the (interlayer) A -site. For Barlowite we have calculated the formation energy of interlayer-substituted Barlowite compared to unmodified Barlowite. The results are also shown in Table I. Formation of a substituted compound is always favorable except for mercury (Hg^{2+}).

The doping energies shown in Fig. 2 of the main paper are computed from energy differences between structures with dopant atoms occupying the interlayer sites and structures with dopant atoms on a kagome site (case

TABLE I. Calculated formation and doping energies in eV (electron volts) per formula unit of A -substituted Herbertsmithite $ACu_3(OH)_6Cl_2$ and A -substituted Barlowite $ACu_3(OH)_6FBr$ ($A = Li, Na, Mg, Ca, Zn, Cd, Hg, Sc, Y, Al, Ga, In$). Negative values signal stability of the stoichiometric compound against the formation of Clinoatacamite/Barlowite (case 1), doping into the kagome layer (case 2, see Fig. 2 in main paper), vacancies on the interlayer site (case 3) and impurities on the interlayer site (case 4). Ionic radii in coordination number 6 are taken from Ref. 7. In this configuration Cu^{2+} has an ionic radius of 72 pm.

case	A -Herbertsmithite, $A =$	Li^{1+}	Na^{1+}	Mg^{2+}	Ca^{2+}	Zn^{2+}	Cd^{2+}	Hg^{2+}	Sc^{3+}	Y^{3+}	Al^{3+}	Ga^{3+}	In^{3+}
1	$ACu_3(OH)_6Cl_2$	-2.660	-2.517	-5.333	n/a	-2.082	-1.461	n/a	-7.300	-7.144	-6.257	-2.939	-3.080
2	$ACu_3(OH)_6Cl_2$	-0.041	+0.257	-0.421	n/a	-0.261	+0.128	n/a	-0.372	+0.043	-1.101	-0.736	-0.203
3	$A_{0.66}Cu_3(OH)_6Cl_2$	-0.847	-0.735	-1.689	n/a	-0.694	n/a	n/a	-2.481	-2.398	-2.141	-1.176	-1.062
4	$A_{0.66}Cu_{3.33}(OH)_6Cl_2$	-1.497	-1.350	-2.308	n/a	-1.321	n/a	n/a	-3.019	-2.878	-2.659	-1.711	-1.585
A -Barlowite, $A =$													
1	$ACu_3(OH)_6FBr$	-2.860	-2.247	-5.089	-5.808	-2.074	-1.420	+1.317	-7.498	-7.400	-5.605	-2.895	-2.919
2	$ACu_3(OH)_6FBr$	-0.322	+0.047	-0.994	-0.012	-0.367	+0.183	+1.282	-0.738	-0.336	-0.555	-0.363	-0.276
	ionic radius in pm	76	102	72	100	74	95	102	75	90	54	62	80

2). The values for the doping energies are given in Table I, together with ionic radii taken from Ref. 7.

Having established the stability of stoichiometric compounds, we investigate the solid solution of Zn and Ga dopants. To accommodate non-integer dopant concentrations, we use $2 \times 1 \times 1$ and $3 \times 1 \times 1$ super cells. The formation energy of the target compound having total energy E_T is defined as

$$E_{\text{form}} = E_T + x \cdot (E_{Zn} - E_{Ga}) - (1-x) \cdot E_{ZnH} - x \cdot E_{GaH}, \quad (3)$$

where E_{ZnH} refers to Herbertsmithite and E_{GaH} to Gallium-substituted Herbertsmithite. Note that as a reference energy here we use $(1-x) \cdot E_{ZnH} + x \cdot E_{GaH}$, which is the energy that one obtains if the solid solution were to dissociate spontaneously into Herbertsmithite and Ga-substituted Herbertsmithite. Therefore, formation energies are negative if the solid solution is stable against phase separation. Our results show that the solid solution $Ga_xZn_{1-x}Cu_3(OH)_6Cl_2$ should exist in a broad range of doping ratios (Fig. 1). This opens up the possibility to access the van Hove singularities of the kagome lattice at intermediate doping levels⁸ and possible unconventional superconducting states close to $4/3$ filling⁹.

II. DETAILS ON PREPARATION OF HYPOTHETICAL CRYSTAL STRUCTURES

For all cases discussed in the previous section, crystal structures had to be prepared from a stoichiometric structure of Herbertsmithite⁵ or Barlowite⁶. For Herbertsmithite we started from the rhombohedral unit cell of space group $R\bar{3}m$, containing one formula unit. For Barlowite we start from the unit cell in space group $P6_3/mmc$, containing two formula units.

Therefore, after reducing symmetry to space group $P1$, Herbertsmithite allows for only one possibility to arrange dopant atoms or defects for all compositions investigated here, if the smallest possible supercell is considered.

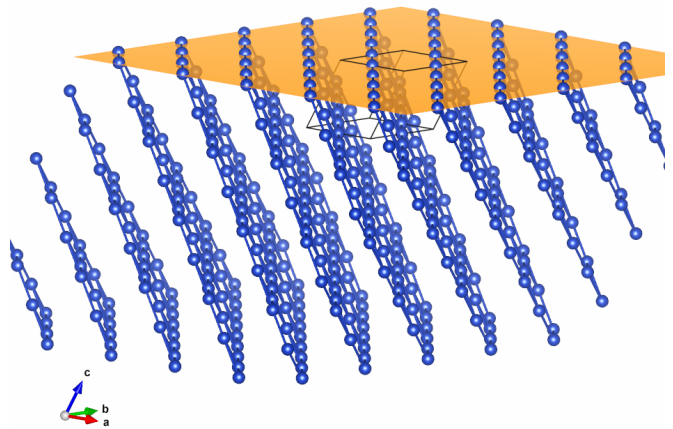


FIG. 2. Cu ions at the (001) surface of Li-Herbertsmithite. Other ions are omitted for clarity. The rhombohedral unit cell is shown in black. Note how all kagome layers are terminated with chains of copper ions at the surface.

For Barlowite, several possibilities of placing defects in the kagome plane exist, because the unit cell already contains two formula units. After reducing symmetry to $P1$, the unit cell contains three copper atoms for each of two different kagome layers stacked in the z -direction. For case 2, where all dopant atoms occupy a kagome site, we choose to place one dopant atom in each kagome layer assuming that clustering is not favored. This reduces the number of defect configurations to two. Either dopant atoms are stacked in the z -direction or placed as far apart as possible, with positioning in the xy -plane alternating between the two kagome layers. We decide for the latter case.

III. FORMALISM FOR COMPUTING SURFACE STATES

We use the Green's function method for the semi-infinite system¹⁰⁻¹² to calculate the states on the (001)

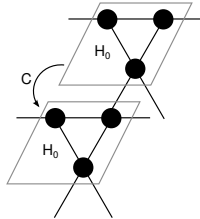


FIG. 3. Schematic picture of the Hamiltonian partitioning in the Green's function method used for calculating the surface states. The principal layer is described by Hamiltonian H_0 , while C contains hopping elements connecting two adjacent principal layers. In the real Herbertsmithite system longer range hoppings are included and two kagome layers belong to one unit cell. For comparison, see Fig. 2.

surface of interlayer substituted Herbertsmithite. In this scheme, the crystal must be partitioned into so-called principal layers parallel to the surface of interest. The Hamiltonian within the principal layer is denoted as H_0 , while the coupling between neighboring principal layers is denoted as C . Note that only hoppings with components in direction either negative or positive perpendicular to the surface must be included into C . The corresponding couplings in the reverse direction are taken into account in the formalism by C^\dagger .

The surface Green's function of a system consisting of N principal layers can be written as

$$G_{ij}^{(N)}(\omega) = \left[\left(\omega - H_0 - CG^{(N-1)}C^\dagger \right)^{-1} \right]_{ij}. \quad (4)$$

The initial condition is

$$G_{ij}^{(1)}(\omega) = (\omega - H_0)_{ij}^{-1}. \quad (5)$$

Indices i, j denote combined site, orbital and spin variables. The Green's function of the dual surface can be calculated by iterating

$$G_{ij}^{(N)}(\omega) = \left[\left(\omega - H_0 - C^\dagger G^{(N-1)}C \right)^{-1} \right]_{ij}. \quad (6)$$

As we use Green's functions on the real-frequency axis, an artificial imaginary part must be added to ensure numerical convergence. To this end, we transform $\omega \rightarrow \omega + i\eta$ with $\eta = 10^{-5}$ eV in the equations above. Although the method in principle allows for the treatment of semi-infinite systems, the numerical iteration of Eq. (4) or (6) has to be stopped with a finite number of layers. We use $N = 10^5$.

IV. (001) SURFACE OF HERBERTSMITHITE

In the main paper we presented topological invariants $\nu_0; (\nu_1, \nu_2, \nu_3) = 0; (111)$ for the Herbertsmithite system. According to Ref. 13, a material with those topological invariants displays conducting states on a (001) surface.

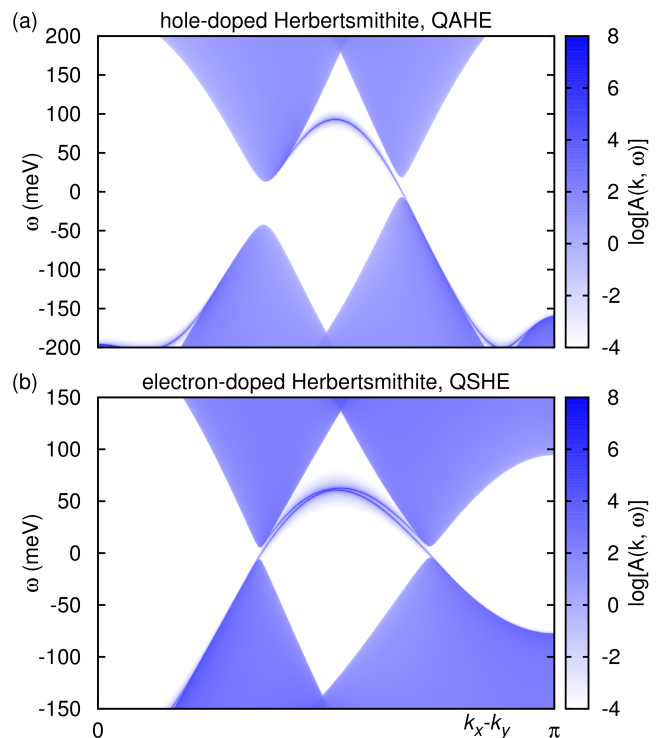


FIG. 4. States on the (001) surface of (a) Li-Herbertsmithite (hole-doped) and (b) Ga-Herbertsmithite (electron-doped) calculated using Green's functions for the semi-infinite system. The kagome layers are terminated with triangles.

The orientation of this lattice plane refers to the unit cell in rhombohedral setting of space group $R\bar{3}m$. The (001) surface of Li-Herbertsmithite is shown in Fig. 2. Note how the Cu ions at the surface are arranged in chains, with all kagome layers terminated equivalently.

The unit cell of (substituted) Herbertsmithite contains in total three Cu ions. These three ions comprise the minimal model of the Herbertsmithite material. In the (001) surface geometry we use, two of the ions are at the surface and one is below the surface. The minimal principal layer therefore comprises Cu ions at different heights within the unit cell. This complicates the partitioning of hopping elements into matrices H_0 and C needed for the Green's function method. The situation is depicted in Fig. 3.

As mentioned in the main paper, and obvious from Fig. 3, the semi-infinite system can be built up either in positive or negative direction perpendicular to the surface. In the kagome lattice this results in an edge termination with either chains or triangles. The case of chains is presented in the main paper. For the dual surface (triangles termination) one obtains a spectral function with equivalent features (see Fig. 4) from Eq. (6).

Both in the main paper and in the supplement we show the spectral function $A(k, \omega)$ only in positive k -direction within the k_x - k_y -plane. As can be seen from Fig. 2, the surface unit cell of (001) Herbertsmithite contains two

TABLE II. Predicted structural parameters for Li-Herbertsmithite $[\text{LiCu}_3(\text{OH})_6\text{Cl}_2]$ ($R\bar{3}m$ space group, $a = 6.96433 \text{ \AA}$, $c = 13.78483 \text{ \AA}$, $Z = 3$).

Atom	Site	x	y	z
Cu	$9d$	$1/2$	0	$1/2$
Li	$3a$	0	0	0
O	$18h$	-0.208833	0.208833	0.447033
H	$18h$	-0.131973	0.131973	0.420633
Cl	$6c$	0	0	0.328170

TABLE III. Predicted structural parameters for Mg-Barlowite $[\text{MgCu}_3(\text{OH})_6\text{FBr}]$ ($P6_3/mmc$ space group, $a = 6.79899 \text{ \AA}$, $c = 9.34513 \text{ \AA}$, $Z = 2$).

Atom	Site	x	y	z
Cu	$6g$	$1/2$	0	0
Mg	$2c$	$1/3$	$2/3$	$1/4$
O	$12k$	0.20346	0.40692	0.09419
H	$12k$	0.12545	0.25090	0.13412
Br	$2d$	$1/3$	$2/3$	$3/4$
F	$2b$	0	0	$1/4$

chains of Cu ions. The surface is mirror symmetric with respect to the k_x and the k_y -direction. Therefore, the symmetry equivalent edge states of the second kagome layer appear in negative k -direction.

V. DETERMINATION OF HEISENBERG HAMILTONIAN PARAMETERS

Based on the theoretically predicted structures of Li-Herbertsmithite [see Table II, Fig. 5 (a)] and Mg-Barlowite [see Table III, Fig. 6 (a)], we use density functional theory calculations to determine the most important couplings of the Heisenberg Hamiltonian. We use the all electron full potential local orbital (FPLO) code¹ with a generalized gradient approximation² exchange and correlation functional and correct for the strong correlations on the Cu^{2+} $3d$ orbitals using GGA+U¹⁴.

The results for $\text{LiCu}_3(\text{OH})_6\text{Cl}_2$ are given in Table IV. The calculation was performed with a $\sqrt{2} \times \sqrt{2} \times 2$ supercell of the rhombohedral primitive cell of Li-Herbertsmithite. With $P1$ symmetry, this cell contains four formula units, *i.e.* twelve inequivalent Cu sites. This allows for 171 out of 4096 unique spin configurations, and the data in Table IV are based on fits to total energies for about 30 of these configurations. The exchange couplings are given assuming $S = 1/2$. However, due to the changed filling of the Cu bands, the moments in the calculation are reduced from $1 \mu_B$ to, on average, about $0.67 \mu_B$. The relevant exchange paths are visualized in Fig. 5 (b). Based on previous work^{15,16}, we consider the GGA+U functional with $U = 6 \text{ eV}$, $J_H = 1 \text{ eV}$ most relevant for Cu in the square planar environment as realized in Herbertsmithite and Barlowite type crystals.

The calculated exchange couplings for

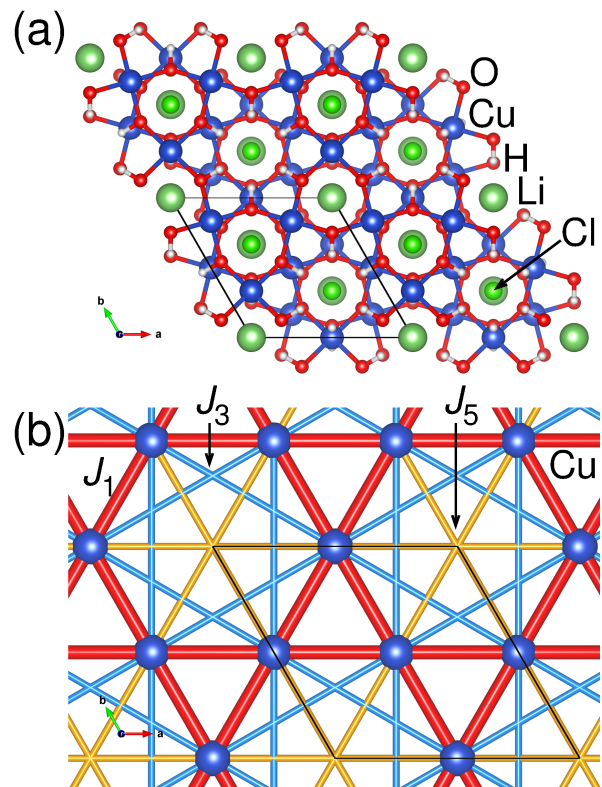


FIG. 5. (a) View of the Li-Herbertsmithite structure along c direction (in hexagonal setting of the $R\bar{3}m$ space group). (b) Detail of the $\text{LiCu}_3(\text{OH})_6\text{Cl}_2$ unit cell with the first three inplane exchange paths between Cu^{2+} ions. Other ions are omitted for clarity.

$\text{MgCu}_3(\text{OH})_6\text{FBr}$ are given in Table V. They are determined using a $\sqrt{2} \times \sqrt{2} \times 1$ unit cell containing four formula units, *i.e.* twelve inequivalent Cu sites. As in the case of $\text{LiCu}_3(\text{OH})_6\text{Cl}_2$, this allows for 171 out of 4096 unique spin configurations. The couplings listed in Table V are based on fits to 25 different spin configurations. As the Cu^{2+} moments are precisely $1 \mu_B$ and all spin configurations lead to gaps of 1.5 eV for $U = 6 \text{ eV}$ and of 2.2 eV for $U = 8 \text{ eV}$, fits are very accurate and the resulting statistical error bars tiny. Only two exchange paths are relevant and are visualized in Fig. 6 (b).

VI. ESTIMATE FOR THE CURIE TEMPERATURE

We estimate the Curie temperature T_C from a simple Weiss mean-field formula¹⁷. For $3d$ transition metals, in this approximation the Curie temperature is given by Eq. (7), where z_i is the coordination number and J_i are the exchange couplings in Kelvin ($U = 6 \text{ eV}$), taken from Table IV.

$$T_C = -\frac{2}{3}S(S+1) \sum_i z_i J_i \quad (7)$$

TABLE IV. Calculated exchange couplings for the theoretically predicted Li-Herbertsmithite, $\text{LiCu}_3(\text{OH})_6\text{Cl}_2$. A GGA+U functional with $J_H = 1$ eV and the two listed U values was used in combination with fully localized limit double counting correction.

U (eV)	J_1 (K)	J_2 (K)	J_3 (K)	J_5 (K)	J_6 (K)
6.0	-544(29)	7(15)	39(24)	-50(13)	2(8)
8.0	-332(32)	-13(16)	-11(27)	-75(20)	1(8)

TABLE V. Calculated exchange couplings for the theoretically predicted Mg-Barlowite, $\text{MgCu}_3(\text{OH})_6\text{FBr}$. A GGA+U functional with $J_H = 1$ eV and the two listed U values was used in combination with fully localized limit double counting correction.

U (eV)	J_1 (K)	J_2 (K)	J_3 (K)	J_4 (K)	J_5 (K)	J_6 (K)	J_7 (K)
6.0	226(1)	13.4(6)	0.0(4)	1.2(4)	-1.0(4)	0.1(3)	-0.3(2)
8.0	167(1)	10.0(4)	0.1(2)	0.4(3)	-0.8(2)	0.0(2)	-0.2(1)

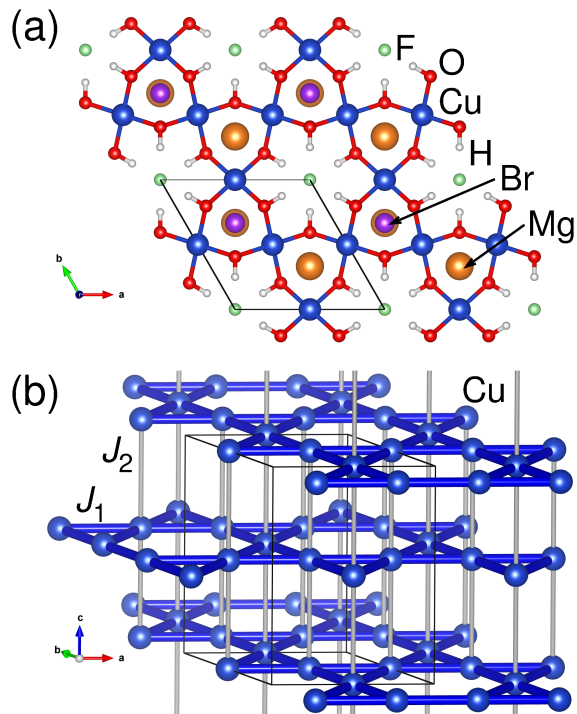


FIG. 6. (a) View of the Mg-Barlowite structure along c direction. (b) Detail of the $\text{MgCu}_3(\text{OH})_6\text{FBr}$ unit cell with the first two exchange paths between Cu^{2+} ions. Other ions are omitted for clarity.

We obtain $T_C = 1160$ K, where we took into account $i = \{1, 3, 5\}$ with $z_i = \{4, 4, 6\}$. Instead of the spin-1/2 model used here, it is also conceivable to parametrize the Heisenberg model with DFT effective moments for S , which would result in a higher value for T_C .

* guterding@itp.uni-frankfurt.de

- ¹ K. Koepf and H. Eschrig, *Full-potential nonorthogonal local-orbital minimum-basis band-structure scheme*, Phys. Rev. B **59**, 1743 (1999); <http://www.FPLO.de>
- ² J. P. Perdew, K. Burke, and M. Ernzerhof, *Generalized Gradient Approximation Made Simple*, Phys. Rev. Lett. **77**, 3865 (1996).
- ³ P. E. Blöchl, *Projector augmented-wave method*, Phys. Rev. B **50**, 17953 (1994).
- ⁴ J. Enkovaara, C. Rostgaard, J. J. Mortensen *et al.*, *Electronic structure calculations with GPAW: a real-space implementation of the projector augmented-wave method*, J. Phys.: Condens. Matter **22**, 253202 (2010); <https://wiki.fysik.dtu.dk/gpaw>
- ⁵ M. P. Shores, E. A. Nytko, B. M. Bartlett, and D. G. Nocera, *A Structurally Perfect $S=1/2$ Kagomé Antiferromagnet*, J. Am. Chem. Soc. **127**, 13462 (2005).
- ⁶ P. Elliott and M. A. Cooper, *Barlowite, $\text{Cu}_4\text{FBr}(\text{OH})_6$, a new mineral isostructural with claringbullite: description and crystal structure*, Mineralog. Mag. **78**, 1755 (2014).
- ⁷ R. D. Shannon, *Revised Effective Ionic Radii and Systematic Studies of Interatomic Distances in Halides and Chalcogenides*, Acta Cryst. A **32**, 751 (1976).
- ⁸ T. Hanisch, G. Uhrig, and E. Müller-Hartmann, *Lattice dependence of saturated ferromagnetism in the Hubbard model*, Phys. Rev. B **56**, 13690 (1997).
- ⁹ I. I. Mazin, H. O. Jeschke, F. Lechermann, H. Lee, M. Fink, R. Thomale, and R. Valentí, *Theoretical prediction of a strongly correlated Dirac metal*, Nat. Commun. **5**, 4261 (2014).
- ¹⁰ M. P. López Sancho, J. M. López Sancho, and J. Rubio, *Quick iterative scheme for the calculation of transfer matrices: application to $\text{Mo}(100)$* , J. Phys. F: Met. Phys. **14**, 1205 (1984).
- ¹¹ M. P. López Sancho, J. M. López Sancho, and J. Rubio, *Highly convergent schemes for the calculation of bulk and surface Green functions*, J. Phys. F: Met. Phys. **15**, 851 (1985).
- ¹² X. Dai, T. L. Hughes, X.-L. Qi, Z. Fang, and S.-C. Zhang, *Helical edge and surface states in HgTe quantum wells and bulk insulators*, Phys. Rev. B **77**, 125319 (2008).
- ¹³ L. Fu and C. L. Kane, *Topological insulators with inversion symmetry*, Phys. Rev. B **76**, 045302 (2007).
- ¹⁴ A. I. Liechtenstein, V. I. Anisimov, and J. Zaanen, *Density-functional theory and strong interactions: Orbital ordering in Mott-Hubbard insulators*, Phys. Rev. B **52**, R5467(R) (1995).
- ¹⁵ H. O. Jeschke, F. Salvat-Pujol, and R. Valentí, *First-principles determination of Heisenberg Hamiltonian parameters for the spin-1/2 kagome antiferromagnet $\text{ZnCu}_3(\text{OH})_6\text{Cl}_2$* , Phys. Rev. B **88**, 075106 (2013).
- ¹⁶ H. O. Jeschke, F. Salvat-Pujol, E. Gati, N. H. Hoang, B. Wolf, M. Lang, J. A. Schlueter, and R. Valentí, *Barlowite as a canted antiferromagnet: theory and experiment*, Phys. Rev. B **92**, 094417 (2015).
- ¹⁷ S. Blundell, *Magnetism in Condensed Matter* (Oxford University Press, Oxford, 2010).